Axions and other WISPs

Dieter Horns[1], *Andreas Ringwald*[2], *Le Hoang Nguyen*[1], *Andrei Lobanov*[1,3]

[1]Institut für Experimentalphysik, Universität Hamburg, Germany
[2]DESY, Hamburg, Germany
[3]Max-Planck-Institut für Radioastronomie, Bonn, Germany

DOI: http://dx.doi.org/10.3204/PUBDB-2018-00782/C1

The project C1 of the SFB 676 concentrated on very weakly interacting slim (i.e., ultra-light) particles (WISPs). The possible occurrence of particular WISP examples such as axions or hidden photons in well-motivated extensions of the Standard Model (SM) was explored. It was shown that WISPs are natural dark matter candidates. Extensive phenomenological, astrophysical, and cosmological studies were performed and WISP experiments were proposed and carried out.

1 Introduction

There are many proposed dark matter particle candidates, spanning a wide parameter range in masses and couplings. Two classes stand out because of their convincing physics case and the variety of experimental and observational probes: WIMPs (Weakly Interacting Massive Particles), such as neutralinos in the minimal supersymmetric standard model (MSSM), and WISPs [1], such as the axion in models solving the strong CP problem. Another candidate is a hidden photon – a new Abelian gauge boson mixing kinetically with the photon. Axions, axion-like particles (ALPs), and hidden photons (HPs) occur naturally in extensions of the SM occurring from string compactifications, cf. Sec. 2. Stars are very efficient sources of WISPs. Therefore, strong constraints on WISPs arise from stellar cooling considerations, cf. Sec. 3. Photons and WISPs may oscillate into each other when propagating through the interstellar and intergalactic medium. This propagation effects may modify photon spectra from astrophysical sources, cf. Sec. 4. Bosonic WISPs are naturally produced in the early universe via the vacuum-realignment mechanism and behave as cold dark matter, cf. Sec. 5. There are several promising techniques to search for WISPs in terrestrial experiments, cf. Sec. 6.

2 WISPs from well-motivated UV completions of the SM

2.1 SM – Axion – Seesaw – Higgs portal inflation (SMASH)

One prominent example of a WISP is the axion [2, 3] – the particle excitation of the phase of a complex scalar field (dubbed Peccei–Quinn field) which gets a vacuum expectation value from the spontaneous breaking of a global chiral $U(1)_{\rm PQ}$ symmetry canceling the CP-violating θ-term in the QCD Lagrangian and thus solving the strong CP problem [4]. In Ref. [5], a minimal extension of the Standard Model (SM) was constructed by adding three right-handed

SM-singlet neutrinos and a vector-like quark, all of them being charged under a global lepton number and Peccei–Quinn (PQ) U(1) symmetry which is spontaneously broken by the vacuum expectation value $v_\sigma \sim 10^{11}\,\mathrm{GeV}$ of a SM-singlet complex scalar field. It was observed that this model solves many problems of the SM in one stroke – neutrino masses and mixing (by the seesaw mechanism), baryogenesis (by leptogenesis), dark matter (by axions), strong CP problem (by axions). In Refs. [6, 7] it was found, that this model automatically also solves the problem of inflation. Indeed, a linear combination of the Peccei–Quinn scalar and the Higgs represents a viable inflaton candidate if the quartic coupling of the former is small, $\lambda_\sigma \sim 10^{-10}$ and the coupling to the Ricci scalar is bounded from below, $\xi_\sigma \gtrsim 10^{-2}$. The model was dubbed "SMASH" (Standard Model*Axion*Seesaw*Higgs portal inflation). It predicts the dark matter axion mass in the range $30\,\mu\mathrm{eV} \lesssim m_A \lesssim 130\,\mathrm{meV}$. It can be probed decisively by upcoming cosmic microwave background and axion dark matter experiments (cf. Sec. 6). First steps towards a GUT SMASH variant are promising [8].

2.2 WISPs from string compactifications

The low-energy limit of string compactifications yields an effective field theory with promising QCD axion candidates [9–12], or even an 'axiverse' containing a plethora of light ALPs with a logarithmically hierarchical mass spectrum [13]. Reference [14] was devoted to the search for closed string axions and ALPs in IIB string flux compactifications. For natural values of the background fluxes and TeV scale gravitino mass, it was found that the moduli stabilisation mechanism of the LARGE Volume Scenario predicts the existence of a QCD axion candidate with intermediate scale decay constant, $f_a \sim 10^{9-12}\,\mathrm{GeV}$, associated with the small cycles wrapped by the branes hosting the visible sector, plus a nearly massless and nearly decoupled ALP associated with the LARGE cycle. In setups where the visible sector branes are wrapping more than the minimum number of two intersecting cycles, there are more ALPs which have approximately the same decay constant and coupling to the photon as the QCD axion candidate, but which are exponentially lighter, realising an axiverse scenario. Models with additional light ALPs where constructed which may explain some intriguing astrophysical anomalies (cf. Secs. 3 and 4), and could be searched for in the next generation of axion helioscopes and light-shining-through-a-wall experiments (cf. Sec. 6).

Axions and ALPs do not exhaust the WISP candidates from string compactifications. Of particular interest are extra "hidden" U(1) gauge bosons which seem to occur frequently in all three major paradigms for string phenomenology – compactifications of the heterotic string, of type II strings with D-branes, and of F-theory [15–18]. They present a window to very large energy scales, since hidden U(1) gauge bosons can mix kinetically with the visible sector hypercharge U(1) gauge boson, leading to a term of mass dimension four in the low-energy effective Lagrangian [19], $\mathcal{L} \supset -\frac{\chi}{2} F_{\mu\nu} X^{\mu\nu}$, where F (X) is the visible (hidden) sector U(1) field strength. Correspondingly, the dimensionless kinetic mixing parameter χ is not necessarily parametrically small, even if the messengers are ultra-heavy. Moreover, on the mass dimension two level, there is also the possibility of Stückelberg mass mixing between hidden U(1)s and the hypercharge U(1). References [20, 21] investigated the masses and the kinetic mixing of hidden U(1)s in LARGE volume compactifications of IIB string theory. It was found that in these scenarios the hidden photons can be naturally light and that their kinetic mixing with the ordinary electromagnetic photon can be of a size interesting for near future experiments and observations (cf. Sec. 6).

3 WISP constraints and hints from stellar cooling

WISPs are produced in hot astrophysical plasmas and can thus transport energy out of stars. Their couplings with SM particles is bounded by the constraint that stellar lifetimes or energy-loss rates should not conflict with observation [22]. Intriguingly, however, stars in different stages in their evolution, notably red giants, horizontal branch stars, and white dwarfs, show a mild preference for a cooling excess beyond the SM. This exotic cooling could be provided by WISPs, produced in the hot stellar cores and escaping the star. In Ref. [23], the cooling hints were analyzed in terms of ALPs, HPs, minicharged particles, and neutrino anomalous magnetic moments. Among them, the ALP or a massless HP appear to represent the best solution. Interestingly, the hinted ALP parameter space is accessible to the next generation proposed ALP searches, such as ALPS II and IAXO (cf. Sec. 6) and the massless HP requires a multi TeV energy scale of new physics that might be accessible at the LHC. In Ref. [24] it was explored whether the best fit to the cooling anomalies can be obtained in particular axion models. It was found that both a DFSZ-type as well as a KSVZ-type axion/majoron model allow a good global fit to the data, preferring an axion mass around 10 meV. An axion in this mass range can also be the main constituent of dark matter (cf. Sec. 5).

4 ALP constraints from photon $\leftrightarrow$ ALP conversion in astrophysical magnetic fields

The constraints from stellar evolution (see previous section) are necessarily limited to the case of photon-ALP mixing in a *high density environment* where the background plasma influences the two photon-ALP mixing. In the case of photon propagation in the interstellar or intergalactic medium as well as in light-shining through wall experiments in vacuum (cf. Sec. 6), the mixing takes place in well-approximated vacuum conditions. The resulting phenomenology may very well differ from the high density environment in stellar interior [25].

The calculation of the probability of converting a photon into an axion-like particle state $p_{\gamma\leftrightarrow a}$ is based upon the term of the Lagrangian

$$\mathcal{L}_{a\gamma} = -\frac{1}{4} g_{a\gamma} a F_{\mu\nu} \tilde{F}^{\mu\nu} = g_{a\gamma} a \mathrm{E}\cdot\mathrm{B}\,. \tag{1}$$

For a polarized beam of photons with energy E propagating along the z-direction, the linearized set of equations takes the form [26]

$$\left(i\frac{d}{dz} + E + \mathcal{M}_0\right)\begin{pmatrix} A_x(z) \\ A_y(z) \\ a(z) \end{pmatrix} = 0\,. \tag{2}$$

For our purposes, we limit the discussion to the simple case of a homogeneous magnetic field which is oriented along the y-axis ($\mathbf{B} = B_T\hat{\mathbf{e}}_y$; for the more general treatment of the problem [27]). In this case, the matrix is commonly written down in the following form:

$$\mathcal{M}_0 = \begin{pmatrix} \Delta_\perp & \Delta_R & 0 \\ \Delta_R & \Delta_\parallel & \Delta_{a\gamma} \\ 0 & \Delta_{a\gamma} & \Delta_a \end{pmatrix}, \tag{3}$$

the elements $\Delta_\perp = \Delta_{\rm pl} + \Delta_\perp^{CM}$, $\Delta_\parallel = \Delta_{\rm pl} + \Delta_\parallel^{CM}$, $\Delta_{a\gamma} = g_{a\gamma} B_T/2$, $\Delta_a = -m_a^2/(2E)$ describe the expected activity of the medium via Δ_R (Faraday rotation) and the birefringence of the medium via the Cotton–Mouton effect leading to $|\Delta_\perp^{CM} - \Delta_\parallel^{CM}|^2 \propto B_T^2$ [26]. For the photon energies considered here, we can neglect the Δ_R term. The presence of free charges in the plasma with volume number density n_e leads to the characteristic plasma frequency for electrons

$$\omega_{\rm pl} = \sqrt{4\pi\alpha n_e m_e^{-1}} \simeq 1.17 \times 10^{-14} \left(\frac{n_e}{10^{-7}\ {\rm cm}^{-3}}\right)^{0.5}\ {\rm eV}\,. \tag{4}$$

With the given choice of the transverse magnetic field, the polarization amplitudes are either parallel to the magnetic field $A_y(z) = A_\parallel(z)$ or perpendicular $A_x(z) = A_\perp(z)$. The matrix $\mathcal{M}$ describing a decoupled $A_\perp$, while $A_\parallel$ and a are evolving via mixing through the off-diagonal element $\Delta_{a\gamma}$. The solution to the coupled differential equation is obtained via rotation with the angle

$$\tan(2\theta) = \frac{2\Delta_{a\gamma}}{\Delta_{\rm pl} - \Delta_a}, \quad \sin(2\theta) = \frac{2\Delta_{a\gamma}}{\Delta_{\rm osc}}\,. \tag{5}$$

This is a very similar situation to the two-flavor mixing of propagating neutrino states, with the probability of oscillating from one state to the other over a distance d:

$$p_{a\gamma} = p_{\gamma a} = \sin^2(2\theta)\sin^2\left(\frac{\Delta_{\rm osc}\ d}{2}\right), \tag{6}$$

with

$$\Delta_{\rm osc} = \sqrt{(\Delta_a - \Delta_{\rm pl})^2 + 4\Delta_{a\gamma}^2}\,, \tag{7}$$

or re-written with the definition

$$E_c \equiv \frac{E|\Delta_a - \Delta_{\rm pl}|}{2\Delta_{a\gamma}}\,, \tag{8}$$

$$\Delta_{\rm osc} = 2\Delta_{a\gamma}\sqrt{1 + \left(\frac{E_c}{E}\right)^2}\,. \tag{9}$$

The energy E_c basically separates two regimes of photon-ALPs mixing: For $E \ll E_c$, the mixing angle $\theta = \Delta_{a\gamma}/\Delta_{\rm osc} \ll 1$ leads to very inefficient and rapid mixing except for a resonance when $\Delta_a = \Delta_{\rm pl}$. For $E \simeq E_c$, the mixing becomes energy-dependent, while at $E \gg E_c$, the mixing angle $\theta = \pi/4$ leads to maximum mixing without any dependence on the energy.

The range of possible astrophysical observations relating to propagation of photons and effects of photon-ALPs mixing is naturally very wide-reaching. However, the approaches fall typically into three categories:

1. Polarization
2. Disappearance channel
3. Appearance channel

All three approaches have been used within the recent years to interpret observations at various wavelengths including radio/UV (birefringence), high-energy gamma-rays (disappearance channel), and very high energy gamma-rays (appearance channel).

4.1 Polarization/dichroism

The coupling of $A_{\parallel}$ via $\Delta_{a\gamma}$ leads for $\Delta_{\rm osc} d \ll 1$ to a reduction of the polarization of $A_{\parallel}$, while $A_{\perp}$ remains unchanged. Under the assumption that birefringence can be ignored, we can observe a dichroic effect, changing the angle of polarization $\phi(z)$:

$$\phi(z) = \phi_0 + \arctan\left(\frac{A_{\parallel}(z)}{A_{\perp}(z)}\right). \tag{10}$$

We have carried out a study with 8 radio galaxies with measured polarization angle. The sources are located at redshift values between 2.34 and 3.57. The polarization angle is measured with respect to the orientation of the observed radio jet. The observed polarization angles are close to 90 degrees which is expected under the assumption that the emission is produced by electrons in the magnetic field aligned with the jet axis.

Since the magnetic field structure of the intervening medium is not well constrained, a simulation of single domains, randomly aligned with the line of sight is carried out and the resulting distribution of polarization angle changes is compared with the measurement. In a maximum-likelihood method, we were able to constrain $B_T g_{a\gamma} \lesssim 10^{-11}\mathrm{GeV}^{-1}$ nG for ultralight ALPS of $m_a \lesssim 10^{-15}$ eV$\approx \omega_{\rm pl}$. Further details are given in [28].

4.2 Disappearance channel

The mixing of photons and ALPs in a transverse magnetic field leads to the apparent disappearance of photons whenever the distance traveled $d \approx \Delta_{\rm osc}$ and the energy of the photon is $E \gtrsim E_c$. For a typical Galactic magnetic field configuration, large scale and ordered field structures exist aligned with the spiral arms. The halo of the Galaxy is magnetized and the field strength is estimated to be in the range of a few μG. Therefore, the critical energy

$$E_c \simeq 2.5\ \mathrm{GeV}\frac{|m_a^2 - \omega_{\rm pl}^2|}{\mathrm{neV}}\left(\frac{B_T}{\mu\mathrm{G}}\right)^{-1}\left(\frac{g_{a\gamma}}{10^{-11}\ \mathrm{GeV}^{-1}}\right)^{-1}, \tag{11}$$

is within the reach of the *Fermi*-LAT instrument which has been observing the entire gamma-ray sky in the energy range between 100 MeV and several TeV since August 2008. The oscillation length for $E \gg E_c$ is

$$l_{\rm osc} = \frac{2\pi}{\Delta_{\rm osc}/2} \approx 32\ \mathrm{kpc}\left(\frac{B_T}{\mu\mathrm{G}}\right)^{-1}\left(\frac{g_{a\gamma}}{10^{-11}\ \mathrm{GeV}^{-1}}\right)^{-1}. \tag{12}$$

For typical values of the Galactic magnetic field, we can therefore expect to observe conversion and even re-conversion of photons when propagating along a line of sight that intersects spiral arms with a large pitch angle. We have therefore analyzed the energy spectra of suitable sources obtained with *Fermi*-LAT. Since the distance of the objects needs to be known, we focused on Galactic gamma-ray pulsars. The gamma-ray spectra of pulsars share a similar shape (they follow a power-law with an exponential suppression at the high energy end). Furthermore, the well-known and nearby (200 pc) Vela pulsar serves as a calibration source to verify that indeed the spectrum of this object does not show any energy-dependent modulation.

In a recent publication [29], we have demonstrated the method and its application to a sample of six gamma-ray pulsars. The most distant object in the sample PSR J2021+3651 is poorly fit with a standard pulsar spectrum - the residuals indicate structures at GeV-energies

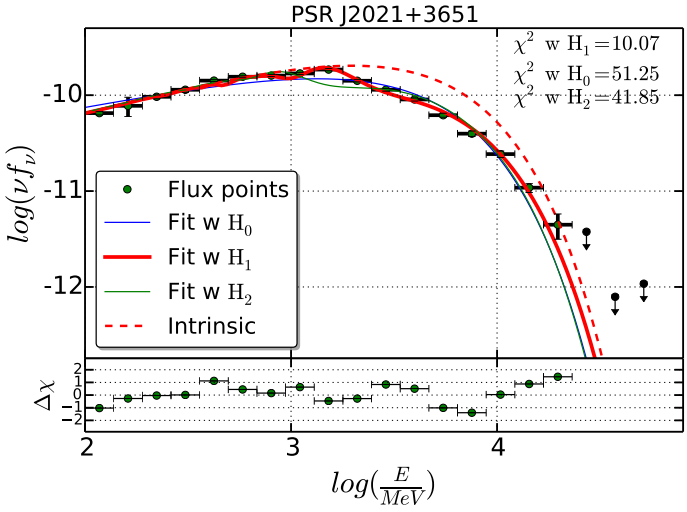

Figure 1: As an example of the studied pulsars' spectra: the spectral energy distribution of PSR J2021+3651, a young gamma-ray pulsar at a distance of ≈ 10 kpc. A smooth power-law with exponential cut-off spectrum (blue line, marked H_0), does not reproduce the spectrum well, while a fit with photon-ALPs coupling (red solid line, marked H_1) provides a significant improvement. The red dashed line indicates the shape of the emitted spectrum. Figure taken from Ref. [30].

which result in a poor fit of a smooth spectrum (see Fig. 1). We have carried out a combined analysis and found an improvement of the spectral fits of all six objects with a combined significance of 4.6 σ for a choice of $m_a = (3.6^{+0.5_{\rm stat}}_{-0.2_{\rm stat}} \pm 0.2_{\rm sys})$ neV and $g_{a\gamma} = (2.3^{+0.3_{\rm stat}}_{-0.4_{\rm stat}} \pm 0.4_{\rm sys}) \times 10^{-11}$ GeV^{-1}. In addition to the six objects in the Galactic plane presented in [29], we have in addition investigated twelve suitable and bright pulsars off the Galactic plane. Even though these sources have very different directions of lines of sight and distances, the resulting improvement of the fit when assuming a photon-ALPs coupling is significant and constrains the parameters in a consistent range (for details, see [30]).

4.3 Appearance channel

In the mixing matrix given in Eqn. 3, the absorption of photons is not considered. For energetic photons ($E = \mathcal{O}(\text{TeV})$), pair-production of photons on the optical/infra-red photons of the extra-galactic medium leads to a suppression of the observed flux for sources at cosmological distances. This process is included in the mixing matrix via an additional term:

$$\mathcal{M} = \mathcal{M}_0 - i\frac{\Gamma}{2}\begin{pmatrix} 1 & 0 & 0 \\ 0 & 1 & 0 \\ 0 & 0 & 0 \end{pmatrix}, \tag{13}$$

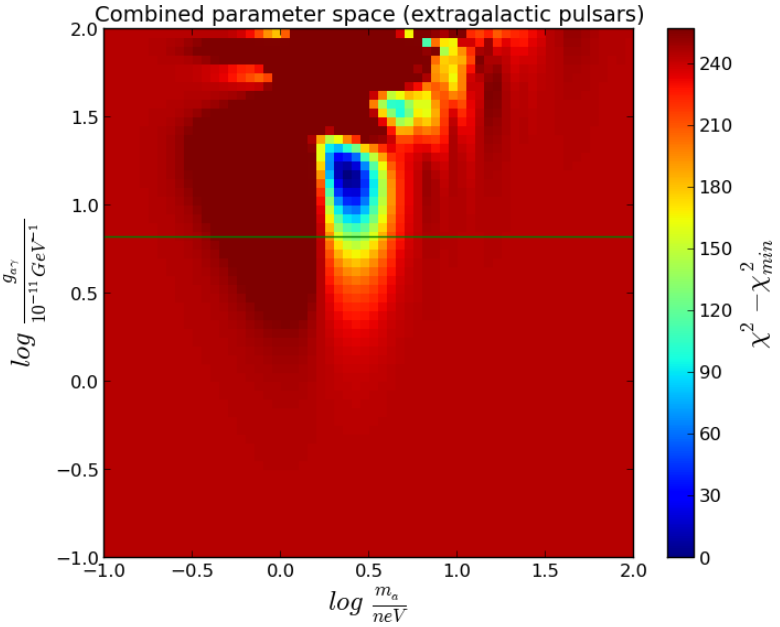

Figure 2: The combination of 12 pulsars located off the Galactic plane: the color-scale indicates the value of $\Delta\chi^2 = \chi^2 - \chi^2_{\rm min}$. For vanishing coupling ($g_{a\gamma} \to 0$), the fit is significantly worse than for the choice of the best-fitting mass m_a and coupling $g_{a\gamma}$ which we estimate to be $m_a \approx 3$ neV and $g_{a\gamma} \approx 10^{-10}$ GeV^{-1}. Figure taken from Ref. [30].

with Γ as the interaction rate calculated from the assumed isotropic background photon field with differential number density $dn = n_{\rm bck}(\epsilon)d\epsilon$:

$$\Gamma(E) = \int\limits_{m_e^2/E}^{\infty} d\epsilon n_{\rm bck}(\epsilon) \int\limits_{-1}^{1-\frac{2m_e^2}{E\epsilon}} d\mu \frac{1-\mu}{2} \sigma_{\gamma\gamma}(\beta)\,, \tag{14}$$

where the cross section above threshold depends on the electron/positron velocity in the center of momentum system $\beta = \sqrt{1 - 2m_e^2(E\epsilon(1-\mu))^{-1}}$:

$$\sigma_{\gamma\gamma} = \sigma_0(1-\beta^2)\left[2\beta(\beta^2-2) + (3-\beta^4)\log\frac{1+\beta}{1-\beta}\right]. \tag{15}$$

At gamma-ray energies, the polarization state is not measured and therefore, the propagated state is described as a density matrix ρ which is propagated across domains of constant magnetic field with random orientation. Further details are discussed in [31].

For the sake of simplicity, we consider the following case similar to the one discussed in [32]: Assuming that the source emits a beam with $a = 0$ and the source is embedded in a region of sufficiently large and turbulent magnetic field (e.g., the intra-cluster medium of a galaxy cluster or group), the photon beam leaving the magnetized source region will be mixed in such a way, that the normalized amplitudes $A_1 + A_2 \approx 2/3$. The beam will propagate through

the intergalactic medium where mixing is rather inefficient given the small magnetic field. However, the photonic part of the beam will get depleted by the absorption by some factor $e^{-\tau}$, where τ is the optical depth $\tau = \Gamma d$. The beam will finally propagate through the Galactic magnetic field, where on average $A_1 + A_2 \approx 2\exp(-\tau)/3 + 1/9$ will be detected. Conversely, once $\tau \gtrsim \ln(6) \approx 1.79$, the additional contribution from the back-converted ALPs-flux starts to dominate over the absorbed flux. Given the monotonic nature of $\Gamma \propto E^{\alpha}$ with $\alpha = -s+1$ for a power-law background field $n_{\rm bck} \propto \epsilon^s$, the effect of *appearance* of gamma-rays subject to large optical depth is most pronounced for sources at large distance and large energies. In a first-time study of the effect and its visibility in gamma-ray spectra from extra-galactic TeV-photon sources, we have demonstrated, that the observed flux above the energy where $\tau(E,z) > 2$ is systematically larger than in the case of a minimum background radiation field [33]. Here, we present an update of that initial analysis, where the data-sample has been expanded and a different method has been used to probe for deviations from the absorption-only picture.

We consider the spectral data-points from the same sample of energy spectra as listed in [34]. For each pair of differential measurements of a source with index j at redshift z_j at energies E_i and $E_{i+1} > E_i$ $f_{ij} = f(E_i, z_j)$ and $f_{i+1,j} = f(E_{i+1}, z_j)$ we calculate the differential slope

$$\alpha_{ij} \equiv \frac{\ln(f_{i+1,j}) - \ln(f_{i,j})}{\ln(E_{i+1}) - \ln(E_i)} = \frac{\Delta \ln(f)}{\Delta \ln(E)} \,. \tag{16}$$

Subsequently, we calculate the average $\langle\alpha\rangle_\tau = \sum w_{ij}\alpha_{ij} / \sum w_{ij}$ where the sum runs over all i, j where τ falls into intervals of width $\Delta\tau$. The averaging takes into account the measurement uncertainties σ_{ij} in an unbiased way via $w_{ij} = \sigma_{ij}^{-2}$. This way, we consider the average slope in bins of optical depth and can analyze the change of α with optical depth. In order to calculate $\tau(E,z)$, a particular model of $n_{\rm bck}$ is used.

The result is shown in Fig. 3 for two different models of the background photon field. The model according to Dominguez [35] is a phenomenological model which provides a prediction of the background field, while the model according to [34] is derived from the gamma-ray spectra (assuming no photon-ALPs mixing). The observed average slope is marked in green while the red points are the calculated slopes $\tilde{\alpha} = (\ln(\tilde{f}_{i+1,j}) - \ln(\tilde{f}_{i,j}))/\Delta\ln(E)$ with $\tilde{f}_{ij} = f_{ij}\ \exp(\tau_{ij})$. In both considered cases, the observed spectra show an upturn for an optical depth of $\tau \gtrsim 1.5$, roughly in line with the expectation considered above. The observed slope hardens monotonically for increasing optical depth. This trend is even more prominent when considering the values of $\tilde{\alpha}$ (red points). For both sets of points a smoothed curve is overlaid to guide the eye. The green shaded region indicates the observable slope that would lead to an intrinsic value of $\tilde{\alpha}$ fixed at the value for optical depth $\tau = 0$. This would be the expectation where the intrinsic slope does not depend on the observed optical depth (the source does not *know*, at which optical depth it is being observed).

In a related study, we have estimated the allowed minimum coupling $g_{a\gamma}$ under the assumption that the magnetic field is not exceeding other bounds [36].

5 WISPy dark matter

It was shown in Ref. [37] that bosonic WISPs, such as ALPs or HPs, are inevitably non-thermally produced in the early universe via the vacuum realignment mechanism and survive as a cold dark matter population until today. It was found that a large part of the parameter range probed by the next generation of experimental WISP searches – exploiting haloscopes (direct

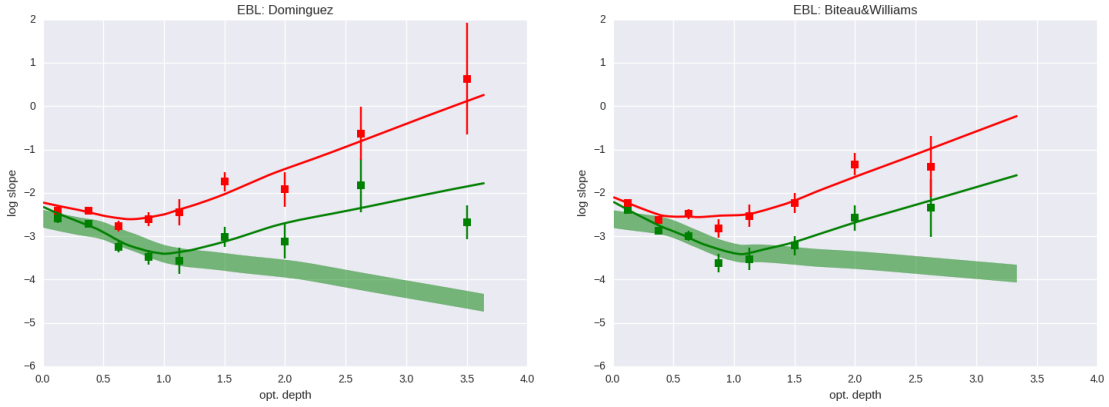

Figure 3: For a sample of extra-galactic TeV sources with redshifts in the range of $z = 0.03 \ldots 1$, the average logarithmic slope of the differential flux measurements (see text for further details) in intervals of optical depth: the green points are the measured (apparent) slopes, while the red points indicate the slopes after correcting for the absorption. In both considered models of the absorbing photon field, an unexpected upturn of slope for optical depth $\tau \gtrsim 1.5$ is apparent that is not expected without an effect related to the propagation of photons. The green shaded region indicates the expected slope of the spectra.

dark matter searches), helioscopes (searches for solar ALPs or HPs), or light-shining-through-a-wall techniques, cf. Sec. 6 – is consistent with the parameter space occupied by WISPy dark matter.

6 WISP searches in terrestrial laboratories

6.1 Light-shining-through-a-wall search: ALPS experiment

The vacuum oscillation of pseudoscalars in vacuum was already introduced in Eqn. (6). In the considered astrophysical settings, the resulting probability is typically $p_{a\leftrightarrow\gamma} \approx 0.5(g_{a\gamma} B_T d)^2 \approx 0.05(B_{T,\mu\mathrm{G}}\ g_{-10}\ d_{\mathrm{kpc}})^2$, with $B_T = B_{T,\mu\mathrm{G}}\ \mu$G, $g_{a\gamma} = g_{-10} \times 10^{-10}$ GeV^{-1}, $d = d_{\mathrm{kpc}}$ kpc. In laboratory settings, the corresponding probability $p_{a\leftrightarrow\gamma} \approx 10^{-13}$ when considering a distance of 10 m with a magnetic field of 10 T. In an experiment where the appearance of light behind a wall is considered, the probability is $p_{\gamma\to\gamma} = p^2_{a\leftrightarrow\gamma} \approx 10^{-26}$ for the re-appearance of light.

This approach was exploited in the pioneering ALPS-experiment [38], which used a single dipole magnet and an optical cavity. The setup reached a sensitivity to detect a re-appearance probability of $\approx 10^{-25}$ with a magnetic field of 5 T and $d = 4$ m, resulting in a sensitivity for a coupling $g_{a\gamma} < 7 \times 10^{-8}$ GeV^{-1}. The successor experiment, planned to start taking data in 2020, will increase the length to almost 100 m and add a cavity for the enhanced recovery of the beam after the wall. The proposed experiment [39] is designed to reach a sensitivity to the coupling $g_{a\gamma}$ improved by a factor of ≈ 3000 compared to the previous setup, covering the range of coupling preferred in the astrophysical scenarios discussed earlier.

6.2 Helioscope: Solar Hidden Photon Search (SHIPS)

The production and release of hidden photons from the sun provides an additional energy-loss mechanism that is globally constrained by the evolution of the sun. A more direct approach is the observation of hidden photons produced in the sun's interior [40]. The kinetic mixing couples this light particle with the normal photon. The Lagrangian density is

$$\mathcal{L} = -\frac{1}{4}F_{\mu\nu}F^{\mu\nu} - \frac{1}{4}X_{\mu\nu}X^{\mu\nu} + \frac{m_\chi^2}{2}X_\mu X^\mu - \frac{\chi}{2}F_{\mu\nu}X^{\mu\nu}, \tag{17}$$

where the angle $\chi \ll 1$ parameterizes the kinetic mixing between the two fields. Inside the sun, the coupling with the plasma modes and absorption need to be considered in order to derive the hidden photon flux at Earth. The resulting spectrum (including both resonant and off-resonant production dominating for photon energies above the maximum plasma frequency $\omega_P^2 = 4\pi\,\alpha\,n_e\,m_e^{-1} \approx 0.3$ keV for the central region of the sun). The resonant production takes place in the layers of the sun where the plasma frequency $\omega_P = \omega$ matches the produced photon frequency ω. The bulk of the emitted power is produced in the layers close to the photosphere where the electron density drops fastest. The hidden photon luminosity of the sun scales with $\chi^2 m_\chi^2$.

So-called *helioscopes* are sensitive to the hidden photon flux. The generic setup consists of an evacuated tube (the density should be sufficiently lowered such that $\omega_P < \omega$ and kinetic mixing takes place in vacuum conditions) and a low-background detector sensitive in the relevant energy range. In the case of the sun, the spectrum is dominated by optical emission such that e.g., a cooled photomultiplier tube can be used. If the diameter of the tube is larger than the diameter of the photosensitive surface of the detector, additional optical elements (e.g., a lens) can be used to increase the collection efficiency.

Such a helioscope experiment was designed, built, and operated at the Hamburg observatory under the name of *SHIPS* (solar hidden photon search) [41, 42]. The experiment took 330 hours of data, pointing the tube to the sun (a similar time was used to estimate the background rate). The limit on the rate of photons generated was $\approx 5 \times 10^{-3}$ s^{-1} which translates into a limit on $\chi m_\chi \lesssim 10^{-10}$ eV for the mass range $10^{-4} \lesssim m_\chi/\mathrm{eV} \lesssim 3$.

6.3 Haloscopes

Experiments which are sensitive to a local (Galactic halo) component of nonbaryonic and aphotic (dark) matter, usually are constructed following the haloscope approach. In the case of the QCD axion [43, 44], the guaranteed coupling to two-photon states via the Primakoff effect leads to detectable signals that can be picked up with a haloscope [45]. The original idea takes advantage of a resonator which enhances the oscillating electromagnetic field produced in a strong and external magnetic field. The resulting signal scales for a fixed dark matter energy density in the halo with the volume of the cavity, the energy density of the external magnetic field, and the quality factor of the resonator. The mode-overlap with the oscillating field is usually parameterized with a form-factor which in the ideal case is close to unity, for further details see, e.g., [46].

The resonant frequency ω is determined by the dimension of the cavity: in the case of a pill-box cavity with radius R, the most important $TM_{0,1,0}$ mode has a frequency $\omega \approx 2.405\,cR^{-1} \approx 72$ GHz R_{cm}^{-1}, with $R = R_{\mathrm{cm}}$ cm. The quality factor of a cavity is given by the ratio of its volume to the product of surface and skin depth. The latter scales with $\omega^{-1/2}$. Therefore,

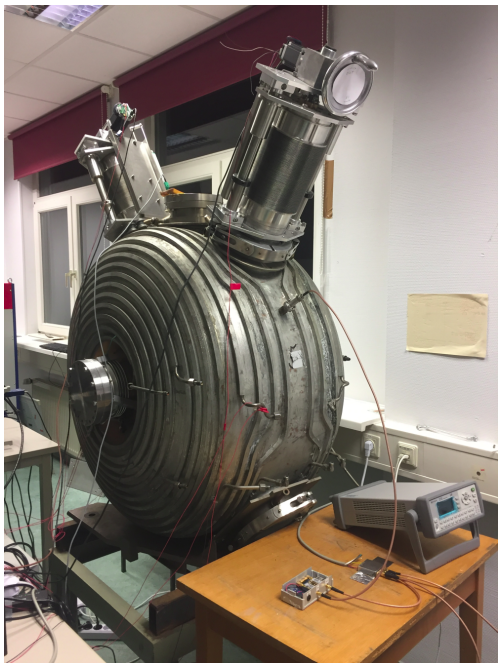

Figure 4: A photo of the WISPDMX setup including the two plunging tuners mounted on top of the cavity. The setup is operated at room temperature.

power generated in a haloscope increases non-linearly with decreasing frequency (or mass of the WISP) (roughly with $R^{7/2}$). This in turn makes it more difficult to detect axions with large mass as compared to smaller masses.
On the other hand, for an axion-haloscope, the entire volume needs to be filled with a strong magnetic field, leading to a fast rise of the expenses when constructing large volume bore magnets. For hidden photon searches however, the measurable power of the cavity does not depend on external magnetic fields. Therefore, hidden-photon haloscopes with large volume detectors are feasible and reach favorable sensitivity.

6.3.1 WISPDMX

Following this notion, we have developed and operated a large cavity experiment (WISPDMX: WISP Dark Matter eXperiment) using a spare resonator cavity of the HERA proton synchrotron accelerator (see Fig. 4). The cavity is operated without a magnetic field and is therefore only sensitive to a hidden-photon type dark matter. The cavity is excited via (neglecting higher order terms in χ)

$$\partial_\mu \partial^\mu A^\nu = m_\chi^2 \, \chi X^\nu, \tag{18}$$

with the field of the hidden photon $|\mathbf{X}| = \rho_{\mathrm{dm}} m_\chi / 2$ related to the local dark matter density $\rho_{\mathrm{dm}} \approx (0.04\ \mathrm{eV})^4$ (in natural units). The resulting power that can be measured with an antenna coupling to the cavity mode with a sub-critical efficiency $\kappa < 0.5$ is then given by

$$\dot{U} = \kappa \, \chi^2 \, m_\chi \, \rho_{dm} \, Q \, V G \,, \tag{19}$$

where G is the form factor of the mode and Q, V are the quality factor and volume of the cavity respectively. When using values characteristic for the WISPDMX setup, we find for the

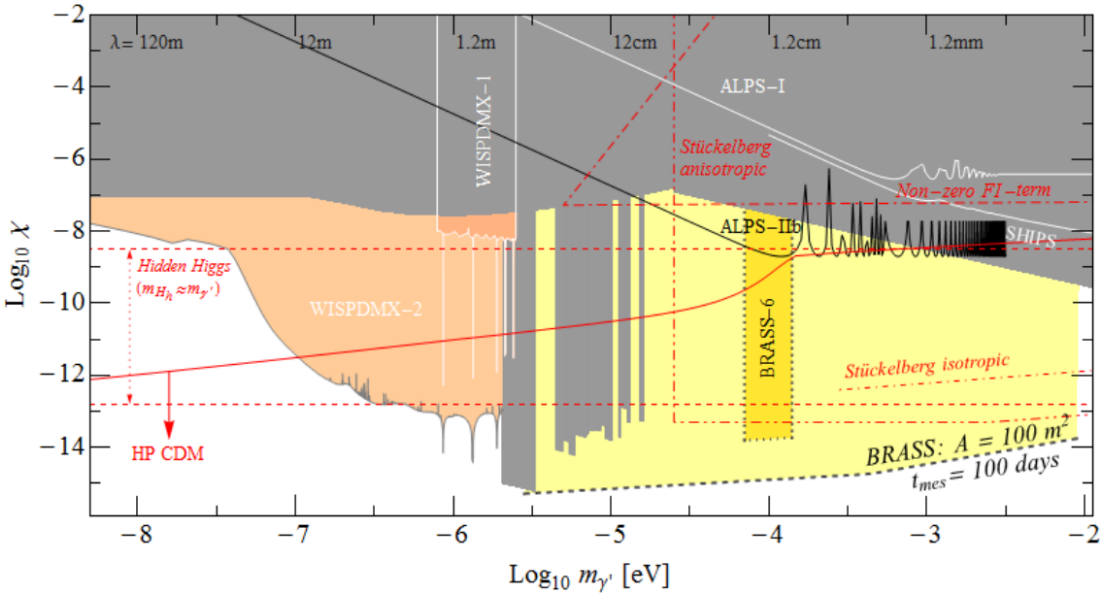

Figure 5: The parameters of mixing χ and mass of the hidden photon m'_γ: The previously existing limits are marked in gray. The preliminary WISPDMX limits are shown in orange. Future limits achievable with the planned non-resonating BRASS experiment are shown in yellow. Theoretically predicted ranges are indicated with red lines.

power (in the case of an isotropic distribution of the vector field $\mathbf{X}$ [47]):

$$\dot{U} \approx 1.63 \times 10^{-16}\ \mathrm{W} \left(\frac{\chi}{10^{-12}}\right)^2 \frac{\kappa}{0.1} \frac{Q}{50\,000} \frac{V}{447\ \mathrm{l}} \frac{G}{0.3} \frac{m_\chi}{\mu\mathrm{eV}} \frac{\rho_0}{\mathrm{GeV\ cm^{-3}}}\,. \tag{20}$$

The experimental setup consists of the cavity, two plunger units for tuning, a set of sensors for temperature, two loop-type antennae, and a low-noise amplification and digitization setup. The setup is operated at room temperature. The amplified signal from the antenna is read-out continuously and streamed to the host computer for 10 seconds via a fast digitizer with 10^9 samples per second. The spectra are then processed in parallel to the next read-out cycle with a GPU card. The system operates nearly in real-time; the resetting of the digitizer card after each cycle leads to a dead time of 4 seconds per cycle. This dead time reduces slightly our sensitivity. We process the spectra with a resolution of 50 Hz per channel. This is sufficient to oversample the expected signal shape at higher frequencies and slightly undersample the signal for lower frequencies.

We have completed the first science run end of 2017. The preliminary result on constraints of the mixing angle χ in the mass range below 2.08 μeV is presented in Fig. 5. The constraints cover a previously unexplored part of the parameter space. The combination of resonant and off-resonant searches demonstrates that a much broader mass range can be constrained with this type of read-out system.

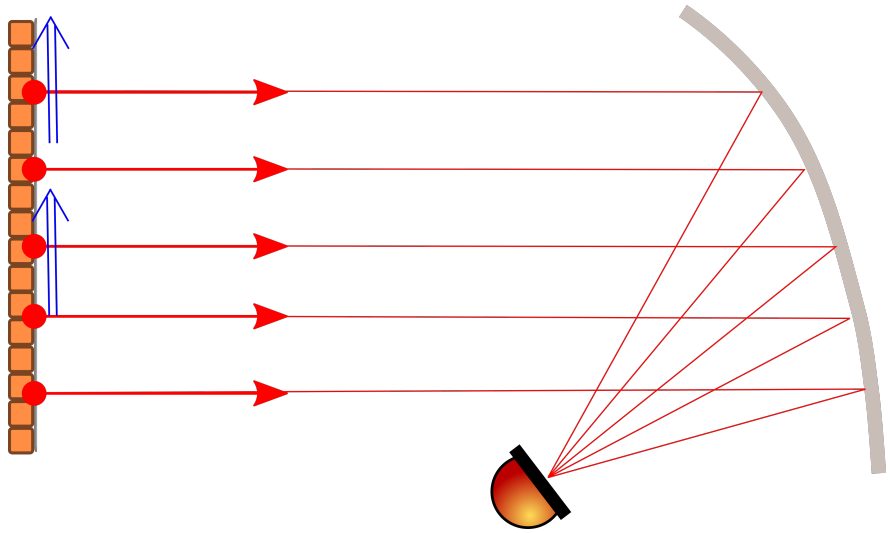

Figure 6: A schematic of the BRASS experiment: The converter surface consist of a layer of permanent magnets arranged in a Halbach-type configuration. The emission is then concentrated via a parabolic reflector into the detection system.

6.3.2 Dish approach

In order to mitigate the inherent problems with cavity-type haloscopes (see the beginning of this section) at high frequencies, a non-resonant approach was suggested [48]. In this approach, the oscillating field at the boundary to a conductor leads to the emission of a propagating wave parallel to the surface normal. This method does not have a resonant enhancement but the large surface area allows to compensate the missing resonance. Also, there is no tuning required and a broad-band search is possible. In this way, we can probe the mass range up to several 100 meV, limited only by the surface quality and detector available. The power radiated of a surface element is given by [48], assuming that the vector dark matter field $\mathbf{X}$ is isotropic:

$$\frac{\dot{U}}{\mathrm{m}^2} = 10^{-23}\ \mathrm{W} \left(\frac{\chi}{2.5 \times 10^{-14}}\right)^2 \frac{\rho_0}{\mathrm{GeV\ cm}^{-3}}\,. \tag{21}$$

In case of a pseudoscalar dark matter field (ALPs or the QCD axion), the dish needs to be magnetized with a predominantly parallel field component $B_\parallel$. The resulting power is therefore [48]:

$$\frac{\dot{U}}{\mathrm{m}^2} = 10^{-23}\ \mathrm{W} \left(\frac{m_a}{0.1\ \mathrm{meV}}\right)^{-2} \frac{\langle B_\parallel^2 \rangle}{\mathrm{T}^2} \left(\frac{g_{a\gamma\gamma}}{10^{-11}\ \mathrm{GeV}^{-1}}\right)^2 \frac{\rho_0}{\mathrm{GeV\ cm}^{-3}}\,. \tag{22}$$

A possible setup of a dish-type haloscope is shown in Fig. 6. In this particular scheme, a surface formed with permanent magnets is used as radiator, illuminating a secondary optic that is viewed by a receiver. A similar scheme is planned for the BRASS experiment.

References

[1] J. Jaeckel and A. Ringwald, *The Low-Energy Frontier of Particle Physics*, *Ann.Rev.Nucl.Part.Sci.* **60** (2010) 405–437, [1002.0329].

[2] S. Weinberg, *A New Light Boson?*, *Phys. Rev. Lett.* **40** (1978) 223–226.

[3] F. Wilczek, *Problem of Strong p and t Invariance in the Presence of Instantons*, *Phys. Rev. Lett.* **40** (1978) 279–282.

[4] R. D. Peccei and H. R. Quinn, *CP Conservation in the Presence of Instantons*, *Phys. Rev. Lett.* **38** (1977) 1440–1443.

[5] A. G. Dias, A. C. B. Machado, C. C. Nishi, A. Ringwald and P. Vaudrevange, *The Quest for an Intermediate-Scale Accidental Axion and Further ALPs*, *JHEP* **06** (2014) 037, [1403.5760].

[6] G. Ballesteros, J. Redondo, A. Ringwald and C. Tamarit, *Unifying Inflation with the Axion, Dark Matter, Baryogenesis, and the Seesaw Mechanism*, *Phys. Rev. Lett.* **118** (Feb, 2017) 071802, [1608.05414].

[7] G. Ballesteros, J. Redondo, A. Ringwald and C. Tamarit, *Standard Model—axion—seesaw—Higgs portal inflation. Five problems of particle physics and cosmology solved in one stroke*, *JCAP* **1708** (2017) 001, [1610.01639].

[8] A. Ernst, A. Ringwald and C. Tamarit, *Axion Predictions in $SO(10) \times U(1)_{\rm PQ}$ Models*, *JHEP* **02** (2018) 103, [1801.04906].

[9] E. Witten, *Some Properties of O(32) Superstrings*, *Phys. Lett.* **149B** (1984) 351–356.

[10] J. P. Conlon, *The QCD axion and moduli stabilisation*, *JHEP* **05** (2006) 078, [hep-th/0602233].

[11] P. Svrcek and E. Witten, *Axions In String Theory*, *JHEP* **06** (2006) 051, [hep-th/0605206].

[12] K.-S. Choi, I.-W. Kim and J. E. Kim, *String compactification, QCD axion and axion-photon-photon coupling*, *JHEP* **03** (2007) 116, [hep-ph/0612107].

[13] A. Arvanitaki, S. Dimopoulos, S. Dubovsky, N. Kaloper and J. March-Russell, *String Axiverse*, *Phys. Rev.* **D81** (2010) 123530, [0905.4720].

[14] M. Cicoli, M. Goodsell and A. Ringwald, *The type IIB string axiverse and its low-energy phenomenology*, *JHEP* **1210** (2012) 146, [1206.0819].

[15] S. A. Abel, J. Jaeckel, V. V. Khoze and A. Ringwald, *Illuminating the Hidden Sector of String Theory by Shining Light through a Magnetic Field*, *Phys. Lett.* **B666** (2008) 66–70, [hep-ph/0608248].

[16] S. A. Abel, M. D. Goodsell, J. Jaeckel, V. V. Khoze and A. Ringwald, *Kinetic Mixing of the Photon with Hidden U(1)s in String Phenomenology*, *JHEP* **07** (2008) 124, [0803.1449].

[17] M. Goodsell and A. Ringwald, *Light Hidden-Sector U(1)s in String Compactifications*, *Fortsch.Phys.* **58** (2010) 716–720, [1002.1840].

[18] M. Goodsell, S. Ramos-Sanchez and A. Ringwald, *Kinetic Mixing of U(1)s in Heterotic Orbifolds*, *JHEP* **1201** (2012) 021, [1110.6901].

[19] B. Holdom, *Two U(1)'s and Epsilon Charge Shifts*, *Phys. Lett.* **166B** (1986) 196–198.

[20] M. Goodsell, J. Jaeckel, J. Redondo and A. Ringwald, *Naturally Light Hidden Photons in LARGE Volume String Compactifications*, *JHEP* **0911** (2009) 027, [0909.0515].

[21] M. Cicoli, M. Goodsell, J. Jaeckel and A. Ringwald, *Testing String Vacua in the Lab: From a Hidden CMB to Dark Forces in Flux Compactifications*, *JHEP* **1107** (2011) 114, [1103.3705].

[22] G. G. Raffelt, *Stars as laboratories for fundamental physics: The astrophysics of neutrinos, axions, and other weakly interacting particles.* University of Chicago Press, Chicago, USA, 1996.

[23] M. Giannotti, I. Irastorza, J. Redondo and A. Ringwald, *Cool WISPs for stellar cooling excesses*, *JCAP* **1605** (2016) 057, [1512.08108].

[24] M. Giannotti, I. G. Irastorza, J. Redondo, A. Ringwald and K. Saikawa, *Stellar Recipes for Axion Hunters*, *JCAP* **1710** (2017) 010, [1708.02111].

[25] J. Jaeckel, E. Masso, J. Redondo, A. Ringwald and F. Takahashi, *The Need for Purely Laboratory-Based Axion-Like Particle Searches*, *Phys. Rev.* **D75** (2007) 013004, [hep-ph/0610203].

[26] G. Raffelt and L. Stodolsky, *Mixing of the photon with low-mass particles*, *Physical Review D* **37** (Mar., 1988) 1237–1249.

[27] A. De Angelis, O. Mansutti, M. Persic and M. Roncadelli, *Photon propagation and the VHE gamma-ray spectra of blazars: how transparent is really the Universe?*, *Mon. Not. Roy. Astron. Soc.* **394** (2009) L21–L25, [0807.4246].

[28] D. Horns, L. Maccione, A. Mirizzi and M. Roncadelli, *Probing axion-like particles with the ultraviolet photon polarization from active galactic nuclei in radio galaxies*, *Phys. Rev.* **D85** (2012) 085021, [1203.2184].

[29] J. Majumdar, F. Calore and D. Horns, *Search for gamma-ray spectral modulations in Galactic pulsars*, *JCAP* **1804** (2018) 048, [1801.08813].

[30] J. Majumdar, *Astrophysical phenomenology of axions and other very weakly interacting sub-eV particles*, Ph.D. thesis, Universität Hamburg, 2018. http://ediss.sub.uni-hamburg.de/volltexte/2018/9220.

[31] A. Mirizzi and D. Montanino, *Stochastic conversions of TeV photons into axion-like particles in extragalactic magnetic fields*, *JCAP* **0912** (2009) 004, [0911.0015].

[32] D. Horns, L. Maccione, M. Meyer, A. Mirizzi, D. Montanino et al., *Hardening of TeV gamma spectrum of AGNs in galaxy clusters by conversions of photons into axion-like particles*, *Phys.Rev.* **D86** (2012) 075024, [1207.0776].

[33] D. Horns and M. Meyer, *Indications for a pair-production anomaly from the propagation of VHE gamma-rays*, *JCAP* **1202** (2012) 033, [1201.4711].

[34] J. Biteau and D. A. Williams, *The extragalactic background light, the Hubble constant, and anomalies: conclusions from 20 years of TeV gamma-ray observations*, *Astrophys. J.* **812** (2015) 60, [1502.04166].

[35] A. Domínguez et al., *Extragalactic Background Light Inferred from AEGIS Galaxy SED-type Fractions*, *Mon. Not. Roy. Astron. Soc.* **410** (2011) 2556, [1007.1459].

[36] M. Meyer, D. Horns and M. Raue, *First lower limits on the photon-axion-like particle coupling from very high energy gamma-ray observation*, *Phys.Rev.* **D87** (2013) 035027, [1302.1208].

[37] P. Arias, D. Cadamuro, M. Goodsell, J. Jaeckel, J. Redondo et al., *WISPy Cold Dark Matter*, *JCAP* **1206** (2012) 013, [1201.5902].

[38] K. Ehret, M. Frede, S. Ghazaryan, M. Hildebrandt, E.-A. Knabbe et al., *New ALPS Results on Hidden-Sector Lightweights*, *Phys.Lett.* **B689** (2010) 149–155, [1004.1313].

[39] R. Bähre et al., *Any light particle search II —Technical Design Report*, *JINST* **8** (2013) T09001, [1302.5647].

[40] J. Redondo and G. Raffelt, *Solar constraints on hidden photons re-visited*, *JCAP* **1308** (2013) 034, [1305.2920].

[41] M. Schwarz, *The Solar Hidden Photon Search (SHIPS)*, Ph.D. thesis, Universität Hamburg, 2015. http://ediss.sub.uni-hamburg.de/volltexte/2015/7320.

[42] M. Schwarz, E.-A. Knabbe, A. Lindner, J. Redondo, A. Ringwald, M. Schneide et al., *Results from the Solar Hidden Photon Search (SHIPS)*, *JCAP* **1508** (2015) 011, [1502.04490].

[43] R. D. Peccei and H. R. Quinn, *CP Conservation in the Presence of Pseudoparticles*, *Physical Review Letters* **38** (June, 1977) 1440–1443.

[44] F. Wilczek, *Problem of Strong P and T Invariance in the Presence of Instantons*, *Physical Review Letters* **40** (Jan., 1978) 279–282.

[45] P. Sikivie, *Experimental Tests of the "Invisible" Axion*, *Physical Review Letters* **51** (Oct., 1983) 1415–1417.

[46] P. Arias, D. Cadamuro, M. Goodsell, J. Jaeckel, J. Redondo and A. Ringwald, *WISPy Cold Dark Matter*, *JCAP* **1206** (2012) 013, [1201.5902].

[47] J. A. R. Cembranos, C. Hallabrin, A. L. Maroto and S. J. N. Jareno, *Isotropy theorem for cosmological vector fields*, *Phys. Rev.* **D86** (2012) 021301, [1203.6221].

[48] D. Horns, J. Jaeckel, A. Lindner, A. Lobanov, J. Redondo et al., *Searching for WISPy Cold Dark Matter with a Dish Antenna*, *JCAP* **1304** (2013) 016, [1212.2970].